

# Tin-Based Perovskite Solar Cells

Subjects: **Energy & Fuels**

Contributor: Syed Afaq Ali Shah , Muhammad Hassan Sayyad , Karim Khan , Kai Guo , Fei Shen , Jinghua Sun , Ayesha Khan Tareen , Yubin Gong , Zhongyi Guo

Since its invention in 2009, Perovskite solar cell (PSC) has attracted great attention because of its low cost, numerous options of efficiency enhancement, ease of manufacturing and high-performance. Within a short span of time, the PSC has already outperformed thin-film and multicrystalline silicon solar cells. A current certified efficiency of 25.2% demonstrates that it has the potential to replace its forerunner generations. However, to commercialize PSCs, some problems need to be addressed. The toxic nature of lead which is the major component of light absorbing layer, and inherited stability issues of fabricated devices are the major hurdles in the industrialization of this technology. Therefore, new researching areas focus on the lead-free metal halide perovskites with analogous optical and photovoltaic performances. Tin being nontoxic and as one of group IV(A) elements, is considered as the most suitable alternate for lead because of their similarities in chemical properties. Efficiencies exceeding 13% have been recorded using Tin halide perovskite based devices. This review summarizes progress made so far in this field, mainly focusing on the stability and photovoltaic performances. Role of different cations and their composition on device performances and stability have been involved and discussed. With a considerable room for enhancement of both efficiency and device stability, different optimized strategies reported so far have also been presented. Finally, the future developing trends and prospects of the PSCs are analyzed and forecasted.

Perovskite Solar Cells (PSCs)

Lead free

Nanomaterial

Photovoltaic , Renewable Energy

## 1. Introduction

For the ever-growing global energy consumption and rapidly depleting fossil fuels reserves, production of energy from clean, sustainable, and renewable energy sources is necessary. Solar radiation is an unlimited form of clean and renewable energy. Its low cost and efficient harvesting can endlessly fuel our civilization. To date, the conventional silicon based solar cells have dominated the photovoltaic (PV) market because of its superior stability and high power conversion efficiency (PCE). Its highest efficiency surpassing 26% recorded at standard test conditions <sup>[1]</sup>. However, the initial production cost associated with silicon wafers used in this technology was very high. Finding alternative technologies to Si solar cells, which can compete in providing high PCE, excellent stability, high reproducibility and low cost, are still challenges for scientific community.

In a short span of less than 10 years, organo-metal halide perovskites (OMHPs) have emerged as a champion photovoltaic technology. Its solution processed fabrication, lower manufacturing cost and high PCE, made perovskite solar cell a promising future photovoltaic technology <sup>[2][3]</sup>. The OMHPs are group of materials with a formula of  $ABX_3$ , where A and B represent cations of different sizes and X represent an anion. For perovskite solar

cell (PSC), the most commonly used small organic-inorganic cations (A), are methyl-ammonium  $\text{CH}_3\text{NH}_3^+$  [4][5], formamidinium  $\text{NH}_2\text{CH}_3\text{NH}_2^+$  [6][7], and cesium Cs [8][9].  $\text{Pb}^{2+}$ ,  $\text{Ge}^{2+}$  and  $\text{Sn}^{2+}$  all belonging to the group-IV(A) family, are widely reported as a divalent metal cation (B) [10][11]. Whereas  $\text{F}^-$ ,  $\text{Cl}^-$ ,  $\text{Br}^-$  and  $\text{I}^-$  are the most used monovalent halogen anions (X) in PSCs [12].

Known for their exceptional optoelectronic properties, perovskite materials were subject of investigation in the late 19<sup>th</sup> century for their potential applications in light emitting diodes (LEDs) and field effect transistors (FETs) [13][14]. In 2009, Miyasaka and coworkers for the first time employed these materials in solar cells [15]. By successfully using of  $\text{CH}_3\text{NH}_3\text{PbBr}_3$  and  $\text{CH}_3\text{NH}_3\text{PbI}_3$  as a sensitizer in Dye-sensitized solar cells (DSSCs), efficiencies of 3.13% and 3.81% were obtained respectively [15]. These efficiencies were further elevated to 6.54% in 2011, when Lee et al., sensitized 3.6  $\mu\text{m}$ -thick  $\text{TiO}_2$  films with quantum dots of  $\text{CH}_3\text{NH}_3\text{PbI}_3$  employing quantum-dot sensitized solar cell (QDSSC) architecture [16]. However, the fabricated devices degraded within minutes because the corrosive redox electrolyte dissolved the QDs. This forced the researchers to focus on all solid state perovskite devices. The very first all solid state perovskite based solar cell was reported in 2012 [17], where the liquid electrolyte was replaced by organic hole transport material, spiro-OMeTAD. This significantly improved the stability of perovskite devices with elevating efficiency to exceed 9% [17]. From then on many notable groups and researchers around the globe joined the perovskite fever [18] by reporting different device architectures such as mesoscopic n-i-p [19], planar n-i-p [20], inverted mesoscopic p-i-n [21] and inverted planar p-i-n [22]. One major factor deciding the performance of the PSC was the quality of perovskite films. To achieve high quality perovskite films many different depositing techniques were reported such as one-step solution deposition [23], two-steps solution deposition [24], vapor assisted deposition [25], thermal vapor deposition [26], blade coating [27], ink jet printing [28], spray coating [29], slot die coating, screen printing and other emerging techniques [30]. To enhance the stability and overall PCE of the devices, many different approaches had been investigated, such as solvent engineering, process engineering, band gap engineering and contact engineering [31].

Within a decade the overall PCE of perovskite solar cell has dramatically improved from 3.81% in 2009 to 25.2% in 2019 [32]. Lead (Pb) was used as a divalent metal cation in almost all high-performance devices [33]. The toxicity of lead is an established fact, and risk of lead being inevitably accumulating in the food chain increases many folds with lead halide making water soluble lead compounds overtime [34]. It is therefore necessary, and compelling to common sense that perovskite solar cells must go lead free. With a smaller ionic radius of 73 (pm), a lower electronegativity and more covalent nature than  $\text{Pb}^{2+}$ ,  $\text{Ge}^{2+}$  was thoroughly investigated by Stoumpos et al., as a potential candidate for replacing lead in PSCs [35]. The germanium perovskites crystallize in trigonal crystal structure having a bandgap of 1.9 eV for  $\text{MAGeI}_3$  [36]. Although the theoretical calculated efficiency for  $\text{CsGeI}_3$  is 27.9% [37], practically the efficiency remained under 1% for all germanium based PSCs because of the poor film quality and instability of the  $\text{Ge}^{2+}$  ion towards oxidation to  $\text{Ge}^{4+}$  [11][35]. Gratzel and group replaced Pb with Cu only to achieve a meager efficiency of 0.017% [38]. High effective mass of holes, low absorption coefficients and the low intrinsic conductivity of the employed perovskite layer proved to be the main causes of poor performance.

Tin (Sn) has emerged as the most promising alternative to lead because of the same isoelectronic configuration of  $\text{s}^2\text{p}^2$ , and has considerably high mobilities [ $10^2\text{-}10^3 \text{ cm}^2(\text{V}^{-1} \text{ s}^{-1})$ ] when used in perovskites as compared to

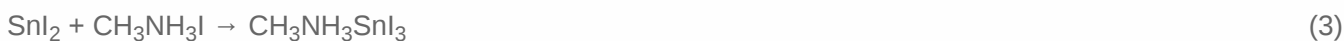
conventional lead based perovskites [ $10\text{-}10^2 \text{ cm}^2 (\text{V}^{-1} \text{ s}^{-1})$ ] [39]. However, the facile formation of Sn vacancies along with stability of Sn in  $2^+$  oxidation state is in question. In the presence of oxygen  $\text{Sn}^{2+}$  is known to be oxidized to  $\text{Sn}^{4+}$  oxidation state [40]. The oxidized  $\text{Sn}^{4+}$  behave as a p-type dopant, and with a concentration of even less than 0.1% it has drastic effects on PCE of the device [41].

Eyeing large scale modules and commercialization of Sn based PSCs, device stability and performance must be addressed simultaneously. Highest efficiencies and highest stabilities reported for Tin based perovskite solar cells having different cations are given below.

## 2. Methylammonium tin halides ( $\text{CH}_3\text{NH}_3\text{SnX}_3$ , X = I, Br, Cl)

In 2014 Snaith and coworkers reported the very first methylammonium tin iodide ( $\text{CH}_3\text{NH}_3\text{SnI}_3$ ) based completely lead free PSC [42]. An efficiency of 6.4% was recorded for the best performing device. The perovskite layer was deposited by spin coating a solution having equimolar quantities of  $\text{CH}_3\text{NH}_3\text{I}$  and  $\text{SnI}_2$  prepared in degassed N-dimethylformamide (DMF). Having a small band gap of 1.23 eV, the open circuit voltage ( $V_{\text{OC}}$ ) for the best performing device showed a remarkable value of 0.88 V, with estimated loss of only 0.35 eV. A mobility of  $1.6 \text{ cm}^2 \text{ V}^{-1} \text{ s}^{-1}$  with diffusion length of 30 nm was calculated for  $\text{CH}_3\text{NH}_3\text{SnI}_3$  perovskite films. While a diffusion length of almost 1  $\mu\text{m}$  was reported for the lead based counterparts of  $\text{MASnI}_3$  [43]. It was observed that for Sn based perovskites the diffusion lengths can be increased up to 1  $\mu\text{m}$  by suppressing background concentration of holes. All devices were fabricated in inert environment and properly encapsulated to minimize the exposure of perovskite layers to oxygen and humidity. While stability of Sn based perovskites remained an issue, high PCE (6.4%) paved the way for further research.

The highest efficiency reported till date for  $\text{MASnI}_3$  based PSCs is 7.78%, achieved through ion exchange/insertion reactions approach [44]. Song and group employed a very unique strategy of using  $\text{SnF}_2$  and MAI as precursors for  $\text{MASnI}_3$  perovskite films through ion exchange/insertion reactions. This unique method resulted in the formation of a very high quality perovskite film, having large amount of  $\text{SnF}_2$  and very low concentration of  $\text{Sn}^{4+}$  [44]. The conversion steps are as follows:



In the very first step of the perovskite film formation an ion exchange reaction took place between gaseous  $\text{CH}_3\text{NH}_3\text{I}$  and a solid state  $\text{SnF}_2$ , generating the intermediate  $\text{SnI}_2$  and byproduct  $\text{CH}_3\text{NH}_3\text{F}$ . The byproduct is then

removed via evaporation in the second step; while in the third step gaseous MAI reacted with  $\text{SnI}_2$  to form the perovskite. It was observed that as the time of ion exchange/insertion reaction was increased from 5 min to 40 min the size of  $\text{MASnI}_3$  crystals also increased forming a compact pinhole free perovskite film. The perovskite films with excess  $\text{SnF}_2$  obtained through this method were used in planer heterojunction structure (ITO/PEDOT:PSS/ $\text{MASnI}_3$ /PC<sub>61</sub>BM/BCP/Ag) PSCs. Champion device produced an overall PCE of 7.78% with a stability of over 200 h for un-encapsulated devices tested under continuous 1 Sun illumination in  $\text{N}_2$  atmosphere. Such a high efficiency with considerable stability is a very promising sign for the future of lead free perovskite devices.

Although, the MA based lead free perovskite devices produced some excellent efficiencies with considerable stability, the lack of control over p-doping has made it very difficult to have high level of reproducibility. Theoretical calculations performed on MA tin based perovskites confirmed that perovskite with MA are more likely to be oxidized than that of perovskites having  $\text{NH}_2\text{CH}_3\text{NH}_2^+$  (FA) as cation [45]. The MA has smaller ionic sizes compared to FA, resulting in a strong antibonding coupling between Sn-s I-p, which consequently results in very high hole densities [46]. In order to have high efficiencies with excellent stability and reproducibility it is therefore necessary to explore other options instead of MA as a cation in lead free perovskite solar cells [47].

### 3. Formamidinium tin halides ( $\text{FASnX}_3$ , X = I, Br, Cl)

The  $\text{MAPbI}_3$  was known to undergo a phase transition at 56 °C, changing its shape from tetragonal to cubic [48]. However, when MA was replaced by  $\text{NH}_2\text{CH}_3\text{NH}_2^+$  (FA), the resulting perovskite  $\text{FAPbI}_3$ , does not show any phase transition until 150 °C. This enhancement of stability can be attributed to a comparatively rigid perovskite structure resulted from enhanced H bonding between organic cation and inorganic matrix [49]. Expecting the same for Sn perovskites, the very first work on formamidinium based tin perovskite was reported by Krishnamoorthy et al., [50] in 2015. An energy band gap of 1.41 eV, with a red shifted absorption onset (880 nm) compared to  $\text{FAPbI}_3$  was observed for  $\text{FASnI}_3$  perovskites. When left overnight, the color of pure  $\text{FASnI}_3$  solution changed from yellow to orange. To solve this issue  $\text{SnF}_2$  was added to the pure  $\text{FASnI}_3$  solution in different molar ratios. Addition of  $\text{SnF}_2$  not only increased the stability but also short circuit current of perovskite devices. The best  $\text{FASnI}_3$  perovskite films were realized with films having 20 mol%  $\text{SnF}_2$ .

Perovskite devices fabricated with these films produced  $J_{\text{SC}}$  of 12.4  $\text{mA.cm}^{-2}$ ,  $V_{\text{OC}}$  of 262 mV, FF of 0.44 and overall PCE of 1.41%. To increase the  $J_{\text{SC}}$  of  $\text{FASnI}_3$  based PSCs Koh and group increased the thickness of mesoporous  $\text{TiO}_2$  from 350 nm to 500 nm [50]. This significantly reduced charge carrier recombinations inside the active material by providing more charge transfer sites. For the best performing device with 500 nm thick mesoporous  $\text{TiO}_2$  layer, a short circuit current density of 24.45  $\text{mA.cm}^{-2}$  was reported with a  $V_{\text{OC}}$  of 238 mV, fill factor of 0.36 and PCE of 2.10% respectively [50]. This pioneering work on  $\text{FASnI}_3$  based perovskite provided a solid reason to explore and further optimize the performance of these devices for environment friendly and stable tin based PSCs. The real push towards a stable and highly efficient FA based tin halide perovskite came from Shin et al., [51] in 2016, when they fabricated a 100 day stable encapsulated perovskite device with a PCE of 4.8% using  $\text{SnF}_2$ -Pyrazine

complex. To achieve this outstanding performance Shin and group deposited the perovskite film using both non solvent dripping process and solvent engineering technique [51].

They demonstrated that  $\text{SnF}_2$  incorporated perovskite films made with only DMF as a solvent showed a very poor surface coverage and morphology. The results were the same even for non-solvent dripping process. But when solvent engineering was applied and films were grown from a mixture of DMF and DMSO in 4:1 volume respectively, a very smooth and uniform film was obtained. However excess  $\text{SnF}_2$  in the  $\text{FASnI}_3$  films caused aggregation on top of film and few plate like aggregates were found on surface. These aggregates disappeared when pyrazine was also introduced along with DMF and DMSO in the solvent mixture. This proved that pyrazine significantly improved the surface morphology by separation of phases induced by excess  $\text{SnF}_2$ . The surface of films prepared with  $\text{SnF}_2$  addition oxidized 100% in air during fabrication process. However,  $\text{Sn}^{4+}$  content decreased in underneath layers. When pyrazine was added to films the oxidation decreased by 4-15% in each layer. When PSCs were fabricated using these optimized perovskite films a  $J_{\text{SC}}$  of  $23.7 \text{ mA.cm}^{-2}$ ,  $V_{\text{OC}}$  of 320 mV, FF of 0.63 and PCE of 4.8% was recorded for the best performing device. These devices showed exceptional reproducibility and long term stability of 100 days in ambient conditions when encapsulated [51].

The real breakthrough for record efficiency in  $\text{FASnI}_3$  based devices was achieved in 2019 when Wu et al., [52] reported a 10.1% efficient device. To obtain a pin hole free film and control the grain boundaries Wu et al., [52] introduced  $\pi$ -conjugated Lewis base molecules during crystallization of  $\text{FASnI}_3$  perovskite films. The precursor solution for the films were prepared mixing 0.1% - 1% in molar ratio, 2-cyano-3-[5-[4-(diphenylamino)phenyl]-2-thienyl]-propenoicacid (CDTA) in DMSO. During film fabrication this additive formed a stable intermediate phase and optimized the crystallization process of perovskite film by significantly slowing down the crystal formation. This method resulted in pin hole free and smooth  $\text{FASnI}_3$  perovskite films with a larger carrier lifetime of 3.87 ns compared to pristine  $\text{FASnI}_3$  film with a carrier lifetime of 2.09 ns. Perovskite devices were fabricated using these films employing ITO/PEDOT:PSS/ $\text{FASnI}_3/\text{C}_60/\text{BCP/Ag}$  architecture. The champion device with an active area of  $0.09 \text{ cm}^2$  yielded record efficiency of 10.17% when 0.2% molar ratio of CDTA was used. The CDTA treatment of the perovskite films enhanced the  $V_{\text{OC}}$  to 0.63 V and FF to 74.7%. When tested for stability, the encapsulated device retained 90% of its initial performance even after 1000 h under continuous light soaking.

## 4. Cesium tin halides ( $\text{CsSnX}_3$ , X = I, Br, Cl)

Kanatzidis and coworkers were the very first to demonstrate effective use of  $\text{CsSnI}_3$  in all solid state DSSC as a hole transport material [53]. The commonly used corrosive redox electrolyte was replaced with  $\text{CsSnI}_3$  to realize efficiencies up to 10.2% in the DSSCs. The first use of  $\text{CsSnI}_3$  as light harvesting material was reported by Wang et al., [54] in 2012, when a simple configuration of ITO/ $\text{CsSnI}_3/\text{Au/Ti}$  produced a PCE of 0.9%. To produce the perovskite film  $\text{SnCl}_2/\text{CsI}$  stack was deposited by e-beam deposition and thermal evaporation of  $\text{CsI}$  and  $\text{SnCl}_2$ , respectively. Followed by annealing at 175 °C for 1 min. This process created a single phased, dense and black colored polycrystalline perovskite film with a grain size of 300 nm. The Schottky solar cell based on these films provided a  $V_{\text{OC}}$  of 0.42 V, with a  $J_{\text{SC}}$  of  $4.80 \text{ mA.cm}^{-2}$ , FF of 22% and PCE of 0.9%.

Kumar et al., were also among the very first researchers who reported the use of  $\text{CsSnI}_3$  in perovskite solar cells [55]. With a band gap close to ideal (1.3 eV) [53] and higher theoretical limit of achievable  $J_{\text{SC}}$  ( $34.3 \text{ mA.cm}^{-2}$ ) than its lead based counterparts ( $25.9 \text{ mA.cm}^{-2}$ ) [56], this material was expected to yield extraordinary efficiencies. However, theoretical calculations revealed that although the material is a semiconductor, it exhibit metallic characteristics with a very high hole mobility arising from intrinsic defects associated with Sn-cation vacancies [57]. To control this metallic conductivity Kumar et al., added  $\text{SnF}_2$  to  $\text{CsSnI}_3$ . Perovskite films were prepared by Stichometric mixing of  $\text{SnI}_2$ ,  $\text{SnF}_2$  and  $\text{CsI}$  in proper solvents followed by spin coating and thermal annealing ( $70^{\circ}\text{C}$ ). Perovskite solar cells employing conventional n-i-p architecture ( $\text{FTO}/\text{c-TiO}_2/\text{mp-TiO}_s/\text{CsSnI}_3+\text{SnF}_2/\text{HTM}/\text{Au}$ ) were fabricated using 4', 4-, 4-tris (N,N-phenyl-3-methylamino) triphenylamine (m-MTDATA) as hole transport material.

To compare performance and effect of  $\text{SnF}_2$  on Sn vacancies,  $\text{CsSnI}_3$  pervoskite films with 0, 5, 10, 20 and 40 mol% of  $\text{SnF}_2$  were used. Devices without any  $\text{SnF}_2$  doping were not functioning at all, while devices with  $\text{SnF}_2$  doping were properly functioning with the best efficiency of 2.02% recorded for device with 20 mol%  $\text{SnF}_2$  doping. These results were further explained by measuring the carrier densities of perovskite films. A very high carrier density of  $10^{19} \text{ cm}^{-3}$  was recorded for pure  $\text{CsSnI}_3$  with holes as majority charge carriers. This p-type conductivity was caused by Sn-vacancies. With increasing mol % of  $\text{SnF}_2$  the carrier densities tend to decrease. This proves that  $\text{SnF}_2$  doping can significantly suppress Sn vacancies. Surprisingly, when stored in glove box these devices were stable for more than 250 h. While these devices show some stability, a very low open circuit voltage hinders the performance of these devices. With an astonishing  $J_{\text{SC}}$  of  $22.70 \text{ mA.cm}^{-2}$  obtained for the best performing device a very low  $V_{\text{OC}}$  of 0.24 V was recorded.

In 2016 Li et al., reported 77 day stable  $\text{CsSnIBr}_2$  films based devices [58]. This extraordinary stability was achieved by adding hypophosphorous acid (HPA) to precursor solution of  $\text{CsSnIBr}_2$  perovskite films. Addition of HPA in precursor solution made tiny clusters of  $\text{CsSnX}_3\text{-HPA}_y$  ( $X = \text{Br, I}$ ). These tiny clusters promoted growth of perovskite crystals by removing the redundant  $\text{SnF}_2$ , hence suppressing phase separation. When films were tested for conductivity, samples prepared with HPA had one order of magnitude less conductivity than those prepared without any HPA addition. Moreover, the charge carrier density reduced by one order of magnitude for films prepared with HPA addition ( $1.5 \times 10^{15} \text{ cm}^{-3}$ ) compared to film prepared without any HPA addition ( $1.6 \times 10^{16} \text{ cm}^{-3}$ ). Overall addition of HPA proved effective in reducing trap densities and Sn vacancies in  $\text{CsSnIBr}_2$  films. The best device was fabricated with  $0.5 \mu\text{L mL}^{-1}$  concentration of HPA acid, presenting efficiency of 3.02% with a  $J_{\text{SC}}$  of  $17.4 \text{ mA.cm}^{-2}$ , a  $V_{\text{OC}}$  of 0.31 V and Fill factor of 56%. When encapsulated these devices retained almost all of their initial performance for a time period of 77 days in ambient conditions. This extraordinary stability with moderate efficiency demonstrated the effective use of  $\text{CsSnIBr}_2$  perovskite layer in lead free stable perovskite devices, paving the way for its commercial applications.

Very recently Li et al., [59] reported one of state-of-the-art performance with a PCE of 3.8% and stability of 180 days. For the very first time vacuum flash-assisted solution processing (VASP) was used to fabricate the high quality  $\text{CsSnI}_3$  perovskite films. The VASP method involved transferring the already spin coated Sn-based perovskite precursor to a vacuum (60 Pa) for 40 s. Followed by annealing at  $60^{\circ}\text{C}$  for 10 min. The controlled

solvent removal method allowed to produce high quality  $\text{CsSnI}_3$  films with very few pin holes, reduced background charge carrier density and considerably enhanced perovskite stability. Films produced by VASP showed greatly improved stability than that of films produced using single step spin coating (controlled films). UV absorption spectrum revealed that at 450 nm VASP films retained 95% of their initial absorption even after 100 min exposure to air, while the controlled film retained only 85.5% absorption. The VASP PSCs yielded a PCE of 2% which increased to 3.8% upon storing in glove box for 3 months. The controlled PSC produced PCE of 1.1% and almost lost all of its performance within the first month of storage.

Over the years a steady progress has been made in elevating the efficiency and enhancing air stability of this single cation (MA, FA, Cs) based Sn perovskites. However, the challenge of commercialization has pushed the scientific and research community to come up with unique ideas. A new trend of combining two or more cations in a single perovskite has emerged, as it offers numerous possibilities of enhancing device performance and stability. This idea proved very successful in lead based perovskites [60][61], simultaneously gaining the attention of groups working on Sn based perovskites. The coming section summarize all work done in this regard based on Sn based perovskite, keeping in view the objective that high efficiency and long term stability should go hand to hand.

## 5. Mix-Cations (MC) tin halides ( $\text{MCSnX}_3$ , X = I, Br, Cl)

Liu and coworkers were the first to report a mixed cation  $(\text{FA})_x(\text{MA})_{1-x}\text{SnI}_3$  perovskite in 2017 [62]. By employing an inverted p-i-n architecture for device fabrication and by optimizing the ratio of both cations within the perovskite layer, a maximum PCE of 8.12% was achieved. By changing the volume ratio x: (1-x) of  $\text{FASnI}_3$  and  $\text{MASnI}_3$  precursor solutions, different mixed cations perovskite layers were obtained with ratios of FA and MA as 0:100, 25:75, 50:50, 75:25 and 100:0 respectively. Perovskite films were realized by a one-step spin coating technique with chlorobenzene and  $\text{SnF}_2$  addition to precursor solution made in DMSO. Bandgap of these films as calculated from photo luminescence (PL) spectra showed an increasing trend with the increase of FA content in films. For the films with FA:MA as 25:75 a bandgap of 1.28 eV was recorded, while for films with FA:MA as 50:50 and 75:25, bandgaps of 1.30 eV and 1.33 eV was recorded respectively. The morphological study of these mixed cation perovskite films revealed that films having lower FA content had few pin holes and low coverage, whereas films with higher FA content,  $(\text{FA})_{0.75}(\text{MA})_{0.25}\text{SnI}_3$  and  $\text{FASnI}_3$  was pin hole free and had complete coverage.

When devices were fabricated incorporating these mixed cations perovskite films a low average PCE of  $3.61\% \pm 0.32\%$  was obtained for  $\text{MASnI}_3$  films. Moreover, with increasing FA content an increase in FF and  $V_{\text{oc}}$  was observed, with the best average PCE of  $7.48\% \pm 0.52\%$  recorded for devices based on  $(\text{FA})_{0.75}(\text{MA})_{0.25}\text{SnI}_3$  perovskite films. The best device based on  $(\text{FA})_{0.75}(\text{MA})_{0.25}\text{SnI}_3$  perovskite films gave maximum efficiency of 8.12% with a  $J_{\text{SC}}$  of  $21.2 \text{ mA.cm}^{-2}$ , a  $V_{\text{OC}}$  of 0.61 V and a FF of 62.7%. This outstanding performance was attributed to the pin hole free and complete coverage of  $(\text{FA})_{0.75}(\text{MA})_{0.25}\text{SnI}_3$  perovskite film. This combination of cations in perovskite significantly reduced the carrier recombination rate as was proved from transient state PL spectra and electrochemical impedance spectroscopy (EIS) of these films.  $(\text{FA})_{0.75}(\text{MA})_{0.25}\text{SnI}_3$  had the highest PL lifetime of  $3.07 \pm 0.1 \text{ ns}$  compared to other mixed cations perovskite films. At high applied voltages the value of  $R_{\text{rec}}$  recorded from EIS was also the largest for this combination among all perovskite films proving the effectiveness of reducing

carrier recombination rate through cation mixing. These devices had a very high reproducibility with considerable stability. Under inert environment these PSCs retained 80% of their initial efficiency for more than 400 h.

Very recently Hayase and group reported the most efficient Sn based PSC with a PCE of more than 13% [63]. To achieve such an outstanding PCE they used two different strategies of efficiency enhancement simultaneously. First of which involved the addition of metals to suppress Sn oxidation, while the second involved the addition of A site cations to control perovskite crystallization. An optimized concentration of EAI was added to the perovskite lattice to favorably align energy bands between the perovskite and charge transport layers. To remove any iodide deficiency in the film  $\text{GeI}_2$  doping was performed, which combined with EAI addition reduced the trap density of the perovskite by 1 order of magnitude. In addition by controlling the amount of EAI in the perovskite lattice the tolerance factor close to 1 was achieved. This proved that this method can be successfully used to produce considerably stable crystal structures.

When devices were fabricated from  $\text{GeI}_2$  doped perovskite employing p-i-n architecture (FTO/PEDOT:PSS/ $\text{GeI}_2$  doped Sn-perovskite/ $\text{C}_{60}$ /BCP/Ag/Au), PCE of 13.24% was achieved with a  $J_{\text{SC}}$  of  $20.32 \text{ mA.cm}^{-2}$ , a  $V_{\text{OC}}$  of 0.84 V and a FF of 78% [63]. This is the highest value of PCE reported for Sn based perovskites till date.

## 6. Conclusion and outlook

Performance and stability of Sn based PSCs is largely depended on perovskite film quality, device architecture and fabrication technique. Optimizing film deposition technique, interface modification and cation substitution have attracted much attention in recent years. Band gap engineering and solvent engineering proved effective in elevating overall PCE and stability of PSCs. Although still lagging in both efficiency and stability when compared to conventional Pb based perovskites, the Sn based counterparts are progressing ever so rapidly. With excellent optical and electrical properties and recent demonstration of efficiency exceeding 13 % the prospect of these perovskites playing a leading role in the future PV market cannot be ruled out. PCE can be significantly improved from the current highest reported efficiencies of 7.78 % [44], 10.17 % [52], 4.81 % [37][64] and 13.24% for  $\text{MASnX}_3$ ,  $\text{FASnX}_3$ ,  $\text{CsSnI}_3$  and  $\text{MCSnX}_3$ , respectively. As the theoretical maximum PCE calculated for  $\text{MASnX}_3$ ,  $\text{FASnX}_3$  and  $\text{CsSnI}_3$  based PSCs is 19.9%, 26.9%, and 25.6% respectively [37]. Based on our thorough analysis, we will provide suggestions on ways to further elevate the PCE and improve stability of tin-based PSCs. Moreover, focusing the commercial applications of Sn based PSCs in building integrated photovoltaics (BIPVs) , suggestions to enhance transparency of PSCs are also provided.

- Minimizing oxygen exposure. One of the major reasons for low performance is  $\text{Sn}^{2+}$  Reducing oxygen exposure during film growth by using techniques such as reducing vapor atmosphere and vacuum growth can significantly improve both efficiency and stability by minimizing p-type doping and enhancing film quality.
- Controlling perovskite crystallization. To reduce density of trap states and optimize charge carrier dynamics different strategies can be used such as introduction of [poly(ethylene-co-vinyl acetate)] [65], pentafluorophenoxyethylammonium iodide (FOEI) [66] or triethylphosphine (TEP) [67] in the perovskite matrix.

- Purification of Sn sources to prevent oxidation. Any commercial  $\text{SnX}_2$  source contains  $\text{Sn}^{4+}$ , even those with 99 % purity contain a significant concentration of oxidized  $\text{Sn}^{4+}$  resulting in poor performance and reproducibility issues [68]. Addition of tin powder can solve this problem by reacting with  $\text{Sn}^{4+}$  and reducing it to  $\text{Sn}^{2+}$
- Inverted p-i-n architecture should be preferred. Better quality of perovskite film can be formed on HTLs by avoiding using salt-doped hole selective layers (HSLs), known to damage Sn perovskite [69][70]. Also p-i-n architecture can favorably align the energy levels of HTL and ETL with perovskite than when used in conventional n-i-p configuration.
- Increasing  $V_{OC}$  by optimizing energy levels. While, the short circuit current ( $J_{SC}$ ) of the PSCs is approaching the theoretical limit, the open circuit voltage ( $V_{OC}$ ) emerges as a major limiting factor for overall performance of Sn based PSCs.  $V_{OC}$  is reduced greatly due to the existence of severe recombination and mismatched energy levels in the device. New techniques of bandgap engineering must be explored along trying more suitable materials as HTL and ETL. For example, Jiang et al., [71] used indene- $\text{C}_{60}$  bisadduct (ICBA) as ETL instead of commonly used PCBM which considerably suppressed the iodide remote doping resulting in a record  $V_{OC}$  of 0.94 V and PCE of 12.4 % with shelf life of more than 3800 h.
- Regulating the A site cation to achieve a tolerance factor of nearly 1. An inverse relation exists between tolerance factor and lattice strain of perovskite crystal. Optimizing A site cation with proper substitution is vital to achieve high performance and stability. Regulating A site cation can make the tolerance factor as close to one as possible, resulting in a stable perovskite structure. For example Nishimura et al., [63] partially substituted formamidinium cation with ethylammonium cation to achieve tolerance factor of 0.9985, achieving record PCE exceeding 13 %.
- Doping Ge in Sn based PSCs. Ge is known to passivate traps and stabilize the mixed 2D/3D perovskite lattice by simultaneously suppressing defect/trap states and  $\text{Sn}^{2+}$  oxidation [72]. The addition of an optimum amount of Ge to develop efficient and stable tin-based PSCs should be an efficient approach.  $\text{Ge}^{2+}$  oxidizes into  $\text{Ge}^{4+}$  resulting in a thin  $\text{GeO}_4$  protecting layer encapsulating tin perovskite crystals. The highest PCE of 13.24 % reported for Sn based PSCs is achieved doping Ge in the perovskite lattice [63].
- Enhancing transparency using bandgap engineering. Halides (Cl, Br, I) play a major role in determining the bandgap of the perovskite. As the halide radii decrease, the bandgap of perovskite increases, allowing more light in the visible region to pass through the perovskite film. For example, the optical bandgap changed from 1.27 eV for pure  $\text{CsSnI}_3$  to 1.37 eV for  $\text{CsSnI}_2\text{Br}$ , and from 1.65 eV for  $\text{CsSnIBr}_2$  to 1.75 eV for  $\text{CsSnBr}_3$ . The increasing bromine content also induced a change in the color of perovskite films from black to light brown, increasing transparency [73].
- Use of transparent contact. Currently most of the fabricated devices use relatively thick ( $\sim 70$  nm or more) metal film as back contact which makes the design opaque. However, a fully semitransparent PSC can be achieved by using 2D structures, transparent conducting oxides (TCOs), graphene electrodes and metal nanowires etc.

Recent progress in the field confirms that Sn based PSCs has great potential for commercialization with very optimistic future prospects. Starting with a PCE of 5.73 % and a shelf life of 12 h, within few years the PCE has exceeded 13% and stability reached 3800 h. With further research and resources directed in this field these nontoxic PSCs will be a major trend of the future.

## References

1. Green, M.A.; Hishikawa, Y.; Dunlop, E.D.; Levi, D.H.; Hohl-Ebinger, J.; Yoshita, M.; Ho-Baillie, A.W.Y. Solar cell efficiency tables (Version 53). *Photovolt. Res. Appl.* 2019, 27, 3–12, doi:10.1002/pip.3102.
2. Lin, J.-T.; Hu, Y.-K.; Hou, C.-H.; Liao, C.-C.; Chuang, W.-T.; Chiu, C.-W.; Tsai, M.-K.; Shyue, J.-J.; Chou, P.-T. Superior Stability and Emission Quantum Yield ( $23\% \pm 3\%$ ) of Single-Layer 2D Tin Perovskite  $\text{TEA}_2\text{SnI}_4$  via Thiocyanate Passivation. *Small* 2020, 16, 2000903, doi:10.1002/smll.202000903.
3. Gao, W.; Li, P.; Chen, J.; Ran, C.; Wu, Z. Interface Engineering in Tin Perovskite Solar Cells. *Mater. Interfaces* 2019, 6, 1901322.
4. Mali, S.S.; Shim, C.S.; Hong, C.K. Highly porous Zinc Stannate ( $\text{Zn}_2\text{SnO}_4$ ) nanofibers scaffold photoelectrodes for efficient methyl ammonium halide perovskite solar cells. *Rep.* 2015, 5, 11424.
5. Mali, S.S.; Shim, C.S.; Hong, C.K. Highly stable and efficient solid-state solar cells based on methylammonium lead bromide ( $\text{CH}_3\text{NH}_3\text{PbBr}_3$ ) perovskite quantum dots. *NPG Asia Mater.* 2015, 7, e208.
6. Xie, F.; Chen, C.-C.; Wu, Y.; Li, X.; Cai, M.; Liu, X.; Yang, X.; Han, L. Vertical recrystallization for highly efficient and stable formamidinium-based inverted-structure perovskite solar cells. *Energy Environ. Sci.* 2017, 10, 1942–1949.
7. Liu, T.; Zhou, Y.; Li, Z.; Zhang, L.; Ju, M.G.; Luo, D.; Yang, Y.; Yang, M.; Kim, D.H.; Yang, W. Stable Formamidinium-Based Perovskite Solar Cells via In Situ Grain Encapsulation. *Energy Mater.* 2018, 8, 1800232.
8. Zhou, W.; Zhao, Y.; Zhou, X.; Fu, R.; Li, Q.; Zhao, Y.; Liu, K.; Yu, D.; Zhao, Q. Light-independent ionic transport in inorganic perovskite and ultrastable Cs-based perovskite solar cells. *Phys. Chem. Lett.* 2017, 8, 4122–4128.
9. Liang, J.; Wang, C.; Wang, Y.; Xu, Z.; Lu, Z.; Ma, Y.; Zhu, H.; Hu, Y.; Xiao, C.; Yi, X. All-inorganic perovskite solar cells. *Am. Chem. Soc.* 2016, 138, 15829–15832.
10. Qin, P.; Tanaka, S.; Ito, S.; Tetreault, N.; Manabe, K.; Nishino, H.; Nazeeruddin, M.K.; Grätzel, M. Inorganic hole conductor-based lead halide perovskite solar cells with 12.4% conversion

efficiency. *Commun.* 2014, 5, 3834.

11. Krishnamoorthy, T.; Ding, H.; Yan, C.; Leong, W.L.; Baikie, T.; Zhang, Z.; Sherburne, M.; Li, S.; Asta, M.; Mathews, N. Lead-free germanium iodide perovskite materials for photovoltaic applications. *Mater. Chem. A* 2015, 3, 23829–23832.

12. Asghar, M.; Zhang, J.; Wang, H.; Lund, P. Device stability of perovskite solar cells—A review. *Sustain. Energy Rev.* 2017, 77, 131–146.

13. Chondroudis, K.; Mitzi, D.B. Electroluminescence from an organic–inorganic perovskite incorporating a quaterthiophene dye within lead halide perovskite layers. *Mater.* 1999, 11, 3028–3030.

14. Mitzi, D.B.; Chondroudis, K.; Kagan, C.R. Organic-inorganic electronics. *IBM J. Res. Dev.* 2001, 45, 29–45.

15. Kojima, A.; Teshima, K.; Shirai, Y.; Miyasaka, T. Organometal halide perovskites as visible-light sensitizers for photovoltaic cells. *Am. Chem. Soc.* 2009, 131, 6050–6051.

16. Im, J.-H.; Lee, C.-R.; Lee, J.-W.; Park, S.-W.; Park, N.-G. 6.5% efficient perovskite quantum-dot-sensitized solar cell. *Nanoscale* 2011, 3, 4088–4093.

17. Kim, H.-S.; Lee, C.-R.; Im, J.-H.; Lee, K.-B.; Moehl, T.; Marchioro, A.; Moon, S.-J.; Humphry-Baker, R.; Yum, J.-H.; Moser, J.E. Lead iodide perovskite sensitized all-solid-state submicron thin film mesoscopic solar cell with efficiency exceeding 9%. *Rep.* 2012, 2, 591.

18. Zhu, X. The Perovskite Fever and Beyond; ACS Publications: Washington, DC, USA, 2016.

19. Heo, J.H.; Im, S.H.; Noh, J.H.; Mandal, T.N.; Lim, C.-S.; Chang, J.A.; Lee, Y.H.; Kim, H.-j.; Sarkar, A.; Nazeeruddin, M.K. Efficient inorganic–organic hybrid heterojunction solar cells containing perovskite compound and polymeric hole conductors. *Photonics* 2013, 7, 486.

20. Zhou, H.; Chen, Q.; Li, G.; Luo, S.; Song, T.-b.; Duan, H.-S.; Hong, Z.; You, J.; Liu, Y.; Yang, Y. Interface engineering of highly efficient perovskite solar cells. *Science* 2014, 345, 542–546.

21. Park, J.H.; Seo, J.; Park, S.; Shin, S.S.; Kim, Y.C.; Jeon, N.J.; Shin, H.W.; Ahn, T.K.; Noh, J.H.; Yoon, S.C. Efficient  $\text{CH}_3\text{NH}_3\text{PbI}_3$  perovskite solar cells employing nanostructured p-type NiO electrode formed by a pulsed laser deposition. *Mater.* 2015, 27, 4013–4019.

22. Dong, Q.; Yuan, Y.; Shao, Y.; Fang, Y.; Wang, Q.; Huang, J. Abnormal crystal growth in  $\text{CH}_3\text{NH}_3\text{PbI}_3-x\text{Cl}_x$  using a multi-cycle solution coating process. *Energy Environ. Sci.* 2015, 8, 2464–2470.

23. Carnie, M.J.; Charbonneau, C.; Davies, M.L.; Troughton, J.; Watson, T.M.; Wojciechowski, K.; Snaith, H.; Worsley, D.A. A one-step low temperature processing route for organolead halide perovskite solar cells. *Commun.* 2013, 49, 7893–7895.

24. Zhao, Y.; Zhu, K. Solution Chem. engineering toward high-efficiency perovskite solar cells. *Phys. Chem. Lett.* 2014, 5, 4175–4186.

25. Hao, F.; Stoumpos, C.C.; Liu, Z.; Chang, R.P.; Kanatzidis, M.G. Controllable perovskite crystallization at a gas–solid interface for hole conductor-free solar cells with steady power conversion efficiency over 10%. *Am. Chem. Soc.* 2014, 136, 16411–16419.

26. Zhao, D.; Ke, W.; Grice, C.R.; Cimaroli, A.J.; Tan, X.; Yang, M.; Collins, R.W.; Zhang, H.; Zhu, K.; Yan, Y. Annealing-free efficient vacuum-deposited planar perovskite solar cells with evaporated fullerenes as electron-selective layers. *Nano Energy* 2016, 19, 88–97.

27. Li, J.; Munir, R.; Fan, Y.; Niu, T.; Liu, Y.; Zhong, Y.; Yang, Z.; Tian, Y.; Liu, B.; Sun, J. Phase Transition Control for High-Performance Blade-Coated Perovskite Solar Cells. *Joule* 2018, 2, 1313–1330.

28. Gribkova, O.L.; Kabanova, V.A.; Tameev, A.R.; Nekrasov, A.A. Ink-Jet Printing of Polyaniline Layers for Perovskite Solar Cells. *Phys. Lett.* 2019, 45, 858–861.

29. Barrows, A.T.; Pearson, A.J.; Kwak, C.K.; Dunbar, A.D.; Buckley, A.R.; Lidzey, D.G. Efficient planar heterojunction mixed-halide perovskite solar cells deposited via spray-deposition. *Energy Environ. Sci.* 2014, 7, 2944–2950.

30. Rong, Y.; Ming, Y.; Ji, W.; Li, D.; Mei, A.; Hu, Y.; Han, H. Toward Industrial-Scale Production of Perovskite Solar Cells: Screen Printing, Slot-Die Coating, and Emerging Techniques. *Phys. Chem. Lett.* 2018, 9, 2707–2713.

31. Song, Z.; Watthage, S.C.; Phillips, A.B.; Heben, M.J. Pathways toward high-performance perovskite solar cells: review of recent advances in organo-metal halide perovskites for photovoltaic applications. *Photonics Energy* 2016, 6, 022001.

32. Green, M.A.; Dunlop, E.D.; Hohlebinger, J.; Yoshita, M.; Kopidakis, N.; Hobaillie, A. Solar cell efficiency tables (Version 55). *Photovolt.* 2020, 28, 3–15.

33. Saliba, M.; Correa-Baena, J.-P.; Wolff, C.M.; Stolterfoht, M.; Phung, N.; Albrecht, S.; Neher, D.; Abate, A. How to Make over 20% Efficient Perovskite Solar Cells in Regular (n–i–p) and Inverted (p–i–n) Architectures. *Mater.* 2018, 30, 4193–4201.

34. Abate, A. Perovskite solar cells go lead free. *Joule* 2017, 1, 659–664.

35. Kopacic, I.; Friesenbichler, B.; Hoefer, S.F.; Kunert, B.; Plank, H.; Rath, T.; Trimmel, G. Enhanced Performance of Germanium Halide Perovskite Solar Cells through Compositional Engineering. *ACS Appl. Energy Mater.* 2018, 1, 343–347, doi:10.1021/acsadmat.8b00007.

36. Stoumpos, C.C.; Frazer, L.; Clark, D.J.; Kim, Y.S.; Rhim, S.H.; Freeman, A.J.; Ketterson, J.B.; Jang, J.I.; Kanatzidis, M.G. Hybrid Germanium Iodide Perovskite Semiconductors: Active Lone

Pairs, Structural Distortions, Direct and Indirect Energy Gaps, and Strong Nonlinear Optical Properties. *Am. Chem. Soc.* 2015, 137, 6804–6819, doi:10.1021/jacs.5b01025.

37. Qian, J.; Xu, B.; Tian, W. A comprehensive theoretical study of halide perovskites  $ABX_3$ . *Electron.* 2016, 37, 61–73.

38. Cortecchia, D.; Dewi, H.A.; Yin, J.; Bruno, A.; Chen, S.; Baikie, T.; Boix, P.P.; Grätzel, M.; Mhaisalkar, S.; Soci, C.; et al. Lead-Free  $MA_2CuCl_xBr_{4-x}$  Hybrid Perovskites. *Chem.* 2016, 55, 1044–1052, doi:10.1021/acs.inorgchem.5b01896.

39. Stoumpos, C.C.; Malliakas, C.D.; Kanatzidis, M.G. Semiconducting tin and lead iodide perovskites with organic cations: phase transitions, high mobilities, and near-infrared photoluminescent properties. *Chem.* 2013, 52, 9019–9038.

40. Abdelaziz, S.; Zekry, A.; Shaker, A.; Abouelatta, M. Investigating the performance of formamidinium tin-based perovskite solar cell by SCAPS device simulation. *Mater.* 2020, 101, 109738.

41. Takahashi, Y.; Hasegawa, H.; Takahashi, Y.; Inabe, T. Hall mobility in tin iodide perovskite  $CH_3NH_3SnI_3$ : evidence for a doped semiconductor. *Solid State Chem.* 2013, 205, 39–43.

42. Noel, N.K.; Stranks, S.D.; Abate, A.; Wehrenfennig, C.; Guarnera, S.; Haghaghirad, A.-A.; Sadhanala, A.; Eperon, G.E.; Pathak, S.K.; Johnston, M.B. Lead-free organic–inorganic tin halide perovskites for photovoltaic applications. *Energy Environ. Sci.* 2014, 7, 3061–3068.

43. Stranks, S.D.; Eperon, G.E.; Grancini, G.; Menelaou, C.; Alcocer, M.J.; Leijtens, T.; Herz, L.M.; Petrozzi, A.; Snaith, H.J. Electron-hole diffusion lengths exceeding 1 micrometer in an organometal trihalide perovskite absorber. *Science* 2013, 342, 341–344.

44. Wang, P.; Li, F.; Jiang, K.; Zhang, Y.; Fan, H.; Zhang, Y.; Miao, Y.; Huang, J.; Gao, C.; Zhou, X. Ion Exchange/Insertion Reactions for Fabrication of Efficient Methylammonium Tin Iodide Perovskite Solar Cells. *Adv. Sci.* 2020, 1903047.

45. Wang, F.; Ma, J.; Xie, F.; Li, L.; Chen, J.; Fan, J.; Zhao, N. Organic Cation-Dependent Degradation Mechanism of Organotin Halide Perovskites. *Funct. Mater.* 2016, 26, 3417–3423.

46. Shi, T.; Zhang, H.-S.; Meng, W.; Teng, Q.; Liu, M.; Yang, X.; Yan, Y.; Yip, H.-L.; Zhao, Y.-J. Effects of organic cations on the defect physics of tin halide perovskites. *Mater. Chem. A* 2017, 5, 15124–15129.

47. Peng, L.; Xie, W. Theoretical and experimental investigations on the bulk photovoltaic effect in lead-free perovskites  $MASnI_3$  and  $FASnI_3$ . *RSC Adv.* 2020, 10, 14679–14688, doi:10.1039/DORA02584D.

48. Baikie, T.; Fang, Y.; Kadro, J.M.; Schreyer, M.; Wei, F.; Mhaisalkar, S.G.; Graetzel, M.; White, T.J. Synthesis and crystal Chem. of the hybrid perovskite  $(CH_3 NH_3)PbI_3$  for solid-state sensitised

solar cell applications. *Mater. Chem. A* 2013, **1**, 5628–5641.

49. Amat, A.; Mosconi, E.; Ronca, E.; Quarti, C.; Umari, P.; Nazeeruddin, M.K.; Grätzel, M.; De Angelis, F. Cation-induced band-gap tuning in organohalide perovskites: interplay of spin–orbit coupling and octahedra tilting. *Nano Lett.* 2014, **14**, 3608–3616.

50. Koh, T.M.; Krishnamoorthy, T.; Yantara, N.; Shi, C.; Leong, W.L.; Boix, P.P.; Grimsdale, A.C.; Mhaisalkar, S.G.; Mathews, N. Formamidinium tin-based perovskite with low  $E_g$  for photovoltaic applications. *Mater. Chem. A* 2015, **3**, 14996–15000.

51. Lee, S.J.; Shin, S.S.; Kim, Y.C.; Kim, D.; Ahn, T.K.; Noh, J.H.; Seo, J.; Seok, S.I. Fabrication of efficient formamidinium tin iodide perovskite solar cells through  $\text{SnF}_2$ –pyrazine complex. *Am. Chem. Soc.* 2016, **138**, 3974–3977.

52. Wu, T.; Liu, X.; He, X.; Wang, Y.; Meng, X.; Noda, T.; Yang, X.; Han, L. Efficient and stable tin-based perovskite solar cells by introducing  $\pi$ -conjugated Lewis base. *China-Chem.* 2020, **63**, 107–115.

53. Lee, B.; He, J.; Chang, R.P.; Kanatzidis, M.G. All-solid-state dye-sensitized solar cells with high efficiency. *Nature* 2012, **485**, 486.

54. Chen, Z.; Wang, J.J.; Ren, Y.; Yu, C.; Shum, K. Schottky solar cells based on  $\text{CsSnI}_3$  thin-films. *Phys. Lett.* 2012, **101**, 093901.

55. Kumar, M.H.; Dharani, S.; Leong, W.L.; Boix, P.P.; Prabhakar, R.R.; Baikie, T.; Shi, C.; Ding, H.; Ramesh, R.; Asta, M. Lead-free halide perovskite solar cells with high photocurrents realized through vacancy modulation. *Mater.* 2014, **26**, 7122–7127.

56. Park, N.-G. Organometal perovskite light absorbers toward a 20% efficiency low-cost solid-state mesoscopic solar cell. *Phys. Chem. Lett.* 2013, **4**, 2423–2429.

57. Chung, I.; Song, J.-H.; Im, J.; Androulakis, J.; Malliakas, C.D.; Li, H.; Freeman, A.J.; Kenney, J.T.; Kanatzidis, M.G.  $\text{CsSnI}_3$ : semiconductor or metal? High electrical conductivity and strong near-infrared photoluminescence from a single material. High hole mobility and phase-transitions. *Am. Chem. Soc.* 2012, **134**, 8579–8587.

58. Li, W.; Li, J.; Li, J.; Fan, J.; Mai, Y.; Wang, L. Additive-assisted construction of all-inorganic  $\text{CsSnI}_3$  mesoscopic perovskite solar cells with superior thermal stability up to 473 K. *Mater. Chem. A* 2016, **4**, 17104–17110.

59. Li, J.; Huang, J.; Zhao, A.; Li, Y.; Wei, M. An inorganic stable Sn-based perovskite film with regulated nucleation for solar cell application. *J. Mater. Chem. C* 2020, **8**, 8840–8845, doi:10.1039/DOTC01800G.

60. Namvar, M.J.; Abbaspour, F.M.H.; Rezaei, R.M.; Behjat, A.; Mirzaei, M. The effect of inserting combined Rubidium-Cesium cation on performance of perovskite solar cell FAMAPb (IBr) 3. *Res.*

Many Body Syst. 2019, 8, 12–142.

61. Zhang, X.; Liu, H.; Wang, W.; Zhang, J.; Xu, B.; Karen, K.L.; Zheng, Y.; Liu, S.; Chen, S.; Wang, K. Hybrid Perovskite Light-Emitting Diodes Based on Perovskite Nanocrystals with Organic–Inorganic Mixed Cations. *Mater.* 2017, 29, 1606405.

62. Zhao, Z.; Gu, F.; Li, Y.; Sun, W.; Ye, S.; Rao, H.; Liu, Z.; Bian, Z.; Huang, C. Mixed-Organic-Cation Tin Iodide for Lead-Free Perovskite Solar Cells with an Efficiency of 8.12%. *Sci.* 2017, 4, 1700204.

63. Nishimura, K.; Kamarudin, M.A.; Hirotani, D.; Hamada, K.; Shen, Q.; Iikubo, S.; Minemoto, T.; Yoshino, K.; Hayase, S. Lead-free tin-halide perovskite solar cells with 13% efficiency. *Nano Energy* 2020, 74, 104858, doi:10.1016/j.nanoen.2020.104858.

64. Song, T.-B.; Yokoyama, T.; Aramaki, S.; Kanatzidis, M.G. Performance enhancement of lead-free tin-based perovskite solar cells with reducing atmosphere-assisted dispersible additive. *ACS Energy Lett.* 2017, 2, 897–903.

65. Liu, G.; Liu, C.; Lin, Z.; Yang, J.; Huang, Z.; Tan, L.; Chen, Y. Regulated Crystallization of Efficient and Stable Tin-Based Perovskite Solar Cells via a Self-Sealing Polymer. *ACS Appl. Mater. Interfaces* 2020, 12, 14049–14056.

66. Meng, X.; Wang, Y.; Lin, J.; Liu, X.; He, X.; Barbaud, J.; Wu, T.; Noda, T.; Yang, X.; Han, L. Surface-Controlled Oriented Growth of FASnI<sub>3</sub> Crystals for Efficient Lead-free Perovskite Solar Cells. *Joule* 2020, 4, 902–912, doi:10.1016/j.joule.2020.03.007.

67. Cao, D.H.; Stoumpos, C.C.; Yokoyama, T.; Logsdon, J.L.; Song, T.-B.; Farha, O.K.; Wasielewski, M.R.; Hupp, J.T.; Kanatzidis, M.G. Thin films and solar cells based on semiconducting two-dimensional ruddlesden–popper (CH<sub>3</sub> (CH<sub>2</sub>)<sub>3</sub>NH<sub>3</sub>)<sub>2</sub> (CH<sub>3</sub>NH<sub>3</sub>)<sub>n-1</sub>Sn<sub>n</sub>I<sub>3n+1</sub> perovskites. *ACS Energy Lett.* 2017, 2, 982–990.

68. Gu, F.; Ye, S.; Zhao, Z.; Rao, H.; Liu, Z.; Bian, Z.; Huang, C. Improving Performance of Lead-Free Formamidinium Tin Triiodide Perovskite Solar Cells by Tin Source Purification. *RRL* 2018, 2, 1800136.

69. Yokoyama, T.; Cao, D.H.; Stoumpos, C.C.; Song, T.-B.; Sato, Y.; Aramaki, S.; Kanatzidis, M.G. Overcoming short-circuit in lead-free CH<sub>3</sub>NH<sub>3</sub>SnI<sub>3</sub> perovskite solar cells via kinetically controlled gas–solid reaction film fabrication process. *Phys. Chem. Lett.* 2016, 7, 776–782.

70. Jung, M.-C.; Raga, S.R.; Qi, Y. Properties and solar cell applications of Pb-free perovskite films formed by vapor deposition. *RSC Adv.* 2016, 6, 2819–2825.

71. Jiang, X.; Wang, F.; Wei, Q.; Li, H.; Shang, Y.; Zhou, W.; Wang, C.; Cheng, P.; Chen, Q.; Chen, L. Ultra-high open-circuit voltage of tin perovskite solar cells via an electron transporting layer design. *Commun.* 2020, 11, 1245.

72. Hayase, S.; Ito, N.; Kamarudin, M.A.K.; Shen, Q.; Ogomi, Y.; Iikubo, S.; Yoshino, K.; Minemoto, T.; Toyoda, T. Pb free perovskite solar cells consisting of mixed metal SnGe perovskite as light absorber. In Proceedings of the Conference Presentation SPIE, San Diego, CA, USA, 18 September 2018.

73. Sabba, D.; Mulmudi, H.K.; Prabhakar, R.R.; Krishnamoorthy, T.; Baikie, T.; Boix, P.P.; Mhaisalkar, S.; Mathews, N. Impact of anionic Br–substitution on open circuit voltage in lead free perovskite ( $\text{CsSnI}_3\text{-xBr x}$ ) solar cells. *Phys. Chem. C* 2015, **119**, 1763–1767.

Retrieved from <https://www.encyclopedia.pub/entry/history/show/6076>